Pol. J. Environ. Stud. Vol. 31, No. 4 (2022), 3941-3953
DOI: *10.15244/pjoes/147099* ONLINE PUBLICATION DATE: 2022-05-17

Original Research

Prediction of Eco-Environmental Vulnerability in Mainland China under the Future Scenarios

Jincai Zhao[1,2], Siying Fan[1], Yaqi Shi[1], Jingyan Feng[1], Zheng Wang[3,4]*

[1]Business School, Henan Normal University, Xinxiang 453007, Henan, China
[2]Research Institute for Rural Revitalization and Common Prosperity, Henan Normal University, Xinxiang 453007, Henan, China
[3]Key Laboratory of Geospatial Technology for the Middle and Lower Yellow River Regions (Henan University), Ministry of Education, 475004, Kaifeng, Henan, China
[4]School of Geographic Sciences, East China Normal University, 200241, Shanghai, China

Received: 8 November 2021
Accepted: 3 March 2022

Abstract

Large-scale eco-environmental vulnerability assessment is conducive to a comprehensive understanding of the quality of ecological environment, which can help accurately capture the ecologically vulnerable areas. Under climate change scenarios, this paper predicted the eco-environmental vulnerability for future mainland China at the county level, and analyzed its trends under the four scenarios. Results shows that areas with higher levels of vulnerability are mainly located in the western China and at the junction of south provinces, while the eco-environmental vulnerability of the eastern and southern coastal areas is relatively low. In terms of temporal trends, the NECR and MGR have the most stable eco-environmental vulnerability, while the eco-environmental vulnerability in the LPR, SWCR and GXR shows an obviously increasing trend under the scenario with high radiative forcing level. The most obvious increase in eco-environmental vulnerability is identified in the North China Plain under RCP 8.5. By comparison, the increment in vulnerability grades during 2020s-2090s is significantly higher than that of the period 2020s-2050s, especially under RCP 8.5 scenario. The trends of eco-environmental vulnerability show upward tendency overall, and the northwestern and southeastern regions have the biggest changes in eco-environmental vulnerability, especially under the high emission scenario.

Keywords: eco-environmental vulnerability, prediction, RCP scenarios, mainland China

Introduction

The geographical and ecological environmental conditions have a significant impact on the survival and development of human beings [1]. The degradation of ecological environment systems would bring about a decline in human well-being [2]. The eco-environmental vulnerability and ecological security have become a more serious geographical and ecological problem influencing sustainable development and management all over the world [3,4]. Rapid industrialization and urbanization have accelerated

*e-mail: wangzheng@casipm.ac.cn

the degree of environmental vulnerability [5, 6], and the global environmentally vulnerable areas have expanded significantly, and the degree of vulnerability has increased significantly [7]. Therefore, reasonable environmental assessment is a critical aspect for sustainable environmental protection and regional development planning [8], especially in areas with high development pressure and high environmental threat [9]. The comprehensive eco-environmental assessment helps to understand the changing process of ecological systems disturbed by the external interference [10], and provides valuable information for the environmental management and protection [11-13]. In the context of global change, global warming significantly affects the terrestrial ecosystem, and the frequency, duration and intensity of the ecological disturbance process also changed [14-16]. More seriously, the frequency and severity of extreme events would increase [17], such as deadly heatwaves [18], drought and extreme rainfall [19, 20], which threaten the survival of human. Therefore, in order to achieve the goal of regional sustainable development, it is of practical significance to assess the eco-environmental vulnerability in the context of global change [21].

Vulnerability assessment from the perspective of climate change mainly focuses on changes in vulnerability in the context of global change, and analyzes the influencing factors of vulnerability to formulate countermeasures to reduce the adverse effect of climate change [22, 23]. Moreover, the conceptual frameworks make vulnerability and risk assessment much clearer [24, 25], such as pressure-state-response framework [26], exposure-sensitivity-adaptive capacity framework [27, 28]. Scholars have paid much attention to the connection between global climate change and ecological vulnerability [29]. For example, Bai et al. [30] selected ten indicators to construct eco-environmental vulnerability, three of which were related to climate change. In addition, extreme climatic events have important impacts on ecosystems and geographical environment [31-34]. With the increase of extreme climate events and the degree of vulnerability, the environment of human settlement also worsens [35]. Droughts and floods would cause damage to property and infrastructure, economic losses, and destruction of ecosystem [36, 37] and threaten the livelihoods of residents. The increasing frequency of extreme climate events reduce agricultural production and livestock production. Studies on vulnerability assessment from the perspective of climate change emerge in large numbers. Mallari [38] selected the influencing factors of climate change on the agricultural sector based on the interview method, and assessed the vulnerability of the agricultural sector during the typhoon in Mabalacat City, Philippines. For vulnerability assessment at the urban scale, Kumar et al. [39] constructed an indicator system under the exposure-sensitivity-adaptability framework. Apreda et al. [40] proposed a method for assessing the impact of extreme weather events on urban systems under the background of climate warming, and the empirical results in eastern area of Naples showed that the method could effectively assess the impacts of heatwaves and flood on climate vulnerability of urban systems. For vulnerability assessment in China, Wang et al. [41] constructed a spatial principal component analysis model including 12 variables of land use, soil erosion, topography, climate, and vegetation, and analyzed the eco-environmental vulnerability and its changes for the Yellow River Basin. Shao et al. [42] selected 9 indexes from the natural and socio-economic aspects, and used the projection pursuit model to examine the ecological vulnerability of the grassland under the background of returning grazing land to grassland. By literature review, it is found that no general rules have been developed for selecting underlying factors in assessing eco-environmental vulnerability to date [13]. Due to the existence of regional differences, the evaluation index systems varied in different regions. Therefore, the regional evaluation results according to the existing research cannot be directly compared spatially. To address the problem, our previous study [43] conducted a comprehensive analysis of the ecological vulnerability of China mainland at the large scale by constructing an evaluation framework including 12 indicators. Nonetheless, this study did not predict the trend of future eco-environmental vulnerability under climate change. Some attempts have been made to map the future vulnerability zones. Wu et al. [44] simulated the future vulnerability of ecosystem throughout the 21st century under the B2 scenario, and results showed that ecosystem is significantly affected by climate change. The impact of climate change in cold regions may be favorable from a near-term perspective. Zhao and Wu [45] employed the data simulated from A2, B2, and A1B scenario to assessed the ecological vulnerability of China in response to future climate change. Results showed that the Northeast and North China are severely affected by climate change and the vulnerable areas expand in the medium and long term, especially in the eastern China. Shukla et al. [46] evaluated the vulnerability of Indian agro-ecological zones to future climate change for RCP scenarios. Uddin et al. [47] mapped the future climate vulnerability of the coastal region of Bangladesh referring to the IPCC framework of vulnerability. Sahoo et al. [48] generated the future environmental vulnerability zones of eastern Dwarakeswar river basin based on the grey-AHP system under RCP 4.5 scenario. Fu et al. [49] conducted an ecological risk assessment for wetland ecosystems in Sanjiang Plain under four RCP scenarios. Xu et al. [50] assessed the vulnerability of ecosystem integrating the effects of temperature and precipitation under RCP 4.5 and 8.5 scenarios in Southwestern China.

However, projection of future environmental vulnerability at national scale is still rarely conducted in the existing literatures. Climate change has a great impact on human production and development

by affecting the agricultural sector; therefore, it is necessary to consider the differences in natural endowments of agricultural zones when assessing the future eco-environmental vulnerability. On this basis, the mainland China was divided into nine agricultural zones. The simulated data under RCP scenarios were used to evaluate the future eco-environmental vulnerability in mainland China. The following paper is organized as follows: Section 2 introduces the data and method used in this study. Section 3 describes temporal and spatial characteristics of indicators related climate change in the future. Section 4 analyzes the future trend and spatial distribution of eco-environmental vulnerability. Section 5 summarizes the research.

Material and Methods

Study Area

According to agricultural planting conditions, the mainland China is divided into nine regions [51]: Gan-Xin Region (GXR), Qinghai-Tibet Plateau Region (QTR), Inner Mongolia and the Great Wall Region (MGR), Northeastern Region (NECR), Loess Plateau Region (LPR), Huang-Huai-Hai Region (HHHR), Southwestern China Region (SWCR), middle and lower regions of the Yangtze River (YRR), Southern China Region (SCR), displayed in Fig. 1.

Data

The data involved in this study include temperature (daily high, low and average temperature), precipitation, wind speed, relative humidity, and leaf area index under four scenarios (RCP 2.6, RCP 4.5, RCP 6.0 and RCP 8.5), all of which come from the Inter-Sectoral Impact Model Inter-comparison Project (ISIMIP), covering from 2006-2099. There are five global climate mode (GCM): MIROC-ESM-CHEM, NorES1-M, IPSL-CM5A-LR, GFDL-ESM2M, and HadGEM2-ES, and their average were used in this study. The bilinear interpolation method was adopted to interpolate the data to a uniform resolution of 0.5°×0.5°, and the statistical deviation correction based on probability distribution was used to correct the interpolated result [52-54].

The effects of global climate change are all-pervasive. The most susceptible factors to climate change are temperature and precipitation, which further disturb snow melt, stream flow [55], agricultural irrigation and land cover [56]. Over the long term, the topography and landform are subject to change. However, changes in topography and landform are much slower than that of meteorological elements. Therefore, the related historical data were used to calculate. Among them, DEM data come from International Scientific & Technical Data Mirror Site, Computer Network Information Center, Chinese Academy of Sciences (http://www.gscloud.cn), with a resolution of 90m. The map of karst landform was vectorized based on the digitized Karst Environment Geological Map of China published by Geology Publishing House. Agricultural irrigation type with a spatial resolution of 10 km was from International Water Management Institute (IWMI).

Fig. 1. Division of nine agricultural zones.

Selection of Indicators

Based on our previous research [43], the evaluation system was constructed from landform, meteorology, vegetation and irrigation, including elevation, bumpiness of land surface (meaning the unevenness of land surface, which is manifested by large slopes, deep trenches, and undulating mountains), karst, frost-free period, extreme high temperature, annual precipitation, drought frequency, flood frequency, wind speed, sunshine hour, vegetation condition and irrigation. Under the climate change scenario, temperature rises significantly, and most areas in Southern China have frost-free period of above 300 days, which cannot fully reflect the difference in the changes of the frost-free period under different RCP scenarios. Therefore, for the future assessment of eco-environmental vulnerability in China, it is reasonable that the frost-free period indicator is replaced by the accumulated temperature, which is defined by the sum of the mean daily temperature exceeding 10ºC in one year. Due to the lack of data, the vegetation condition is represented by the leaf area index (LAI), which means the total one-sided leaf area per unit of land area. LAI is a key indicator for the analysis of physical and biological processes related to the vegetation dynamics at global and regional scales [57].

Table 1. Weights of indicators.

Classification	Index	Direction	Weights
Landform	Elevation	+	0.2067
	Bumpiness of land surface	+	0.1431
	Karst	+	0.1294
Meteorology	Annual precipitation	-	0.0068
	Accumulated temperature	-	0.0198
	Extreme high temperature	+	0.2086
	Drought frequency	+	0.0467
	Flood frequency	+	0.0709
	Wind speed	+	0.0437
	Sunlight hour	-	0.0298
Vegetation coverage	Leaf area index	-	0.0177
Agricultural irrigation	Irrigation index	-	0.0767

The Entropy Method

The entropy method has been proved an objective method to assign a weight to an indicator, and it has been widely used in studies [58]. The detailed mathematical formula could be found in Zhao et al. [43]. This paper takes county as a basic evaluation unit and utilizes the entropy method to calculates the weight for indicators (Table 1).

Mann-Kendall Trend Test and Sen's Slope

The Mann-Kendall (MK) trend test was used in this paper to examine the variation tendency of eco-environmental vulnerability. As a non-parametric test method, it does not require that the data satisfy the assumption of normal distribution, and it is suitable for analyzing time series data with continuous growth or decline (i.e. monotonic trend).

The Sen's slope could effectively quantify the change rate of time series data. For a set of series data $x_i = (x_1, x_2, ..., x_n)$, the Sen's slope is calculated according to Eq. (1).

$$\beta = \text{Median}(\frac{x_j - x_i}{j - i}), \forall j > i \quad (1)$$

where Median is the median function. The positive β means upward trend, and the negative β means downward trend.

Results

Characteristics of Main Indicators

Precipitation

In terms of the regional differences of annual precipitation among the nine agricultural zones in China, the YRR and SCR have the most precipitation, more than twice that of the national average precipitation. The average annual precipitation in SWCR is about 1100 mm, which is relatively high than other regions. The GXR has the minimal annual precipitation, only about 130 mm. The difference in precipitation between the RCP 4.5 and RCP 8.5 scenarios is negligible during 2020-2059, while during 2060-2099, NECR, HHHR and LPR show slight increment in annual precipitation under RCP 8.5 scenario. Compared with the precipitation of these two periods, the average annual precipitation in the second period is obviously more than that of the first period, especially in areas with more annual precipitation, such as YRR, SCR, SWCR.

Accumulated Temperature

There is little difference in spatial distribution of accumulated temperature under the four scenarios. Overall, the Southern China has the highest accumulated temperature, up to more than 5000ºC, followed by the central China, Southeast China and Sichuan Basin, mostly more than 3000ºC. The accumulated temperature in Inner Mongolia and the Northeastern China is relatively low, not exceeding 2000ºC in general. Qinghai-Tibet region has the lowest accumulated temperature, basically lower than 1000ºC. There is an obvious rising trend in accumulated temperature with the rise of radiative forcing level in the Southern China, northwest desert region and north Bohai Bay.

Extreme High Temperature

Taking 35ºC and 38ºC as thresholds respectively, the numbers of days whose daily high temperature is not less than the threshold, called as high temperature days and hot days, are extracted under RCP 2.6 and RCP 8.5 scenarios. The high temperature days are most prominent in the northwestern and southeastern China, where the northwestern China with more high temperature days and the southeastern China with a wider spatial extent. In terms of the hot days, under RCP 2.6 scenario, areas with more than five hot days almost entirely appear in Taklimakan Desert region located in the Gan-Xin region, some of which even hold more than 60 hot days. Under RCP 8.5 scenario, areas with more than five hot days expand, which indicate that the degree of high heat increases. Large areas with hot days exceeding 10 days appear in the southeastern

Table 2. Classification of SPEI.

SPEI	≤-2.0	-1.5 ~ -1.99	-1.0 ~ -1.49	-.99 ~ .99	1.0 ~ 1.49	1.5 ~1.99	≥ 2.0
Classification	Heavy drought	Middle drought	Light drought	Normal	Light flood	Middle flood	Heavy flood
Weight	1	0.7	0.4	0	0.4	0.7	1

China. All these results show that hot days occur more frequently in high CO_2 emission scenarios.

Drought and Flood Frequency

The drought and flood frequency are calculated based on the Standardized Precipitation Index (SPI) in the study of Zhao et al. [43]. However, SPI does not consider the effect of evapotranspiration. Especially in the context of climate change, the rising temperature stimulates the increase in the evapotranspiration. Therefore, the Standardized Precipitation Evapotranspiration Index (SPEI) was used in this paper. Firstly, the Penman-Monteith method was adopted to calculate the evapotranspiration in future China [59], and then the SPEI was constructed [60]. Finally, according to the classification and weight of SPEI (Table 2), the drought and flood frequency were obtained by weighted summation.

The trends of drought frequency differ significantly under the four RCP scenarios. Under RCP 2.6, large areas show downward trend. Under RCP 4.5 scenario, it is obvious that the majority of northern China shows a significant increase. Areas with declining drought frequency mainly appear in the central China. Under RCP 6.0, almost all regions show an upward trend in drought frequency except the small areas of central Sichuan. The maximum growth rate is about 0.8 per decade. Under RCP 8.5, areas with upward trend expand. The growth rates further increase, with the maximum up to 0.9 per decade. Areas with a fast growth are mainly concentrated in northwestern China.

The trends of flood frequency are absolutely different from the drought frequency. Under RCP 2.6, a relatively small area shows an upward trend in the flood frequency, and areas with a downward trend are distributed widely. Under RCP 4.5, an obvious disparity exists between the north and the south of China. The north China mainly shows a significant downward trend in flood frequency, while the south of China primarily exhibits a significant rising trend, with the maximum of growth rate of around 0.2 per decade. Under RCP 6.0, areas with the declining trend expand. Under RCP 8.5, the growth rates of central Sichuan are conspicuous, up to 0.2 per decade. The northern Heilongjiang, Shanxi, Shaanxi, western Henan, Chongqing and southwestern Yunnan also show the rising trend of flood frequency.

Spatial Distribution of Vulnerability Gradation

According to the average values of eco-environmental vulnerability under the four RCP scenarios, vulnerability was divided into five grades by natural break points (Jenks) method: potential, mild, moderate, severe, and extremely severe vulnerability. The division criteria are shown in Table 3.

At National Scale

At national scale, the area of severe vulnerability and extremely severe vulnerability reaches its maximum under RCP 8.5 scenario, with the areal ratios of 22.4% and 29.74%, respectively. The areal ratio of counties with severe and extremely severe vulnerability are both significantly higher than the number ratio of counties, which shows that the severe and extremely severe vulnerability area are mainly distributed in the western China where the county area is much larger than that of the eastern China. The number ratio of counties with moderate vulnerability is also dominant under RCP 8.5, while the areal ratio is relatively low. There was no significant difference in the proportion of areas with moderate vulnerability under the other three scenarios. Areas with moderate vulnerability under RCP 2.6 is slightly dominant, with the areal ratio of 27.43%. The number ratios of mild and potential vulnerability are significantly higher than the areal ratios, which indicated that these two types of vulnerability are mainly distributed in the eastern region with small area. The number ratio of mild vulnerability is the highest under RCP 4.5 (22.01%), while its areal ratio is the highest under RCP 2.6 (16.25%). The number ratio and areal ratio of potential vulnerability are dominant under RCP 2.6, with 29.01% and 10.89% respectively.

From the perspective of spatial distribution (Fig. 2), the eco-environmental vulnerability is higher in the western China than that of eastern China overall.

Table 3. Classification of environmental vulnerability for future China.

Grades	Potential vulnerability	Mild vulnerability	Moderate vulnerability	Severe vulnerability	Extremely severe vulnerability
Standard	≤ 0.1427	≤ 0.1940	≤ 0.2492	≤ 0.3185	> 0.3185

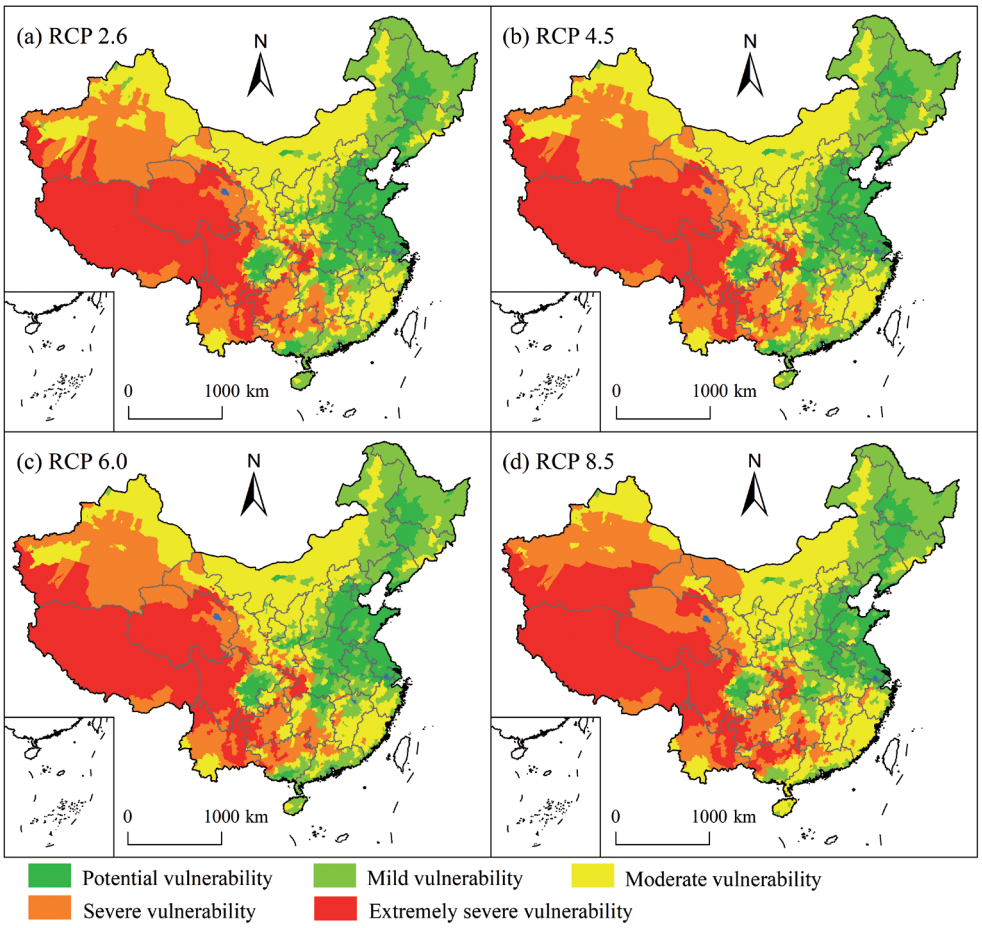

Fig. 2. Maps of eco-environmental vulnerability gradation under RCP scenarios.

Areas with severe and extremely severe vulnerability are mainly distributed in Tibet, Qinghai, western Sichuan and northern Yunnan. Areas with moderate vulnerability are concentrated in northern Xinjiang, Inner Mongolia, Ningxia, northeastern Gansu, Fujian and Zhejiang. Areas with potential and mild vulnerability are mainly located in North China Plain, Sichuan Basin, and southern Guangdong and Guangxi. By comparative analysis among the four RCP scenarios, the Northeast China is the most stable with fewer changes, followed by Inner Mongolia and the Great Wall region. The Loess Plateau, Southwestern China and Gan-Xin regions show more obvious increase in eco-environmental vulnerability under the scenario of high carbon emissions.

On Regional Scale

Comparing the eco-environmental vulnerability among the nine agricultural regions under RCP 2.6 (Fig. 3a), counties with extremely severe vulnerability are mainly distributed in the QTR and SWCR, and the rest small number of counties with extremely severe vulnerability in the YRR, SCR and GXR. About half of counties with severe vulnerability are located in SWCR, and the YRR, SCR, QTR and LPR hold a certain number of counties with severe vulnerability. Areas with moderate vulnerability are distributed in a wide range. Except for the HHHR and QTR, the other seven agricultural areas all have moderate vulnerability areas, of which YRR has the most counties with moderate vulnerability.

To depict the changes in vulnerability of agricultural regions among the four scenarios, this paper makes statistics on the changes in the number of counties with different vulnerability grades under RCP 4.5, 6.0 and 8.5 scenarios compared with that of RCP 2.6 (Fig. 3 (b-f)).

There is a downward trend in the number of counties with potential vulnerability under the three scenarios, and the higher the radiative forcing level, the more obvious the declining trend. By comparing the changes in counties with potential vulnerability among agricultural regions, it can be seen that the number of counties in the YRR and HHHR decreases the most, followed by the LPR and SCR, while the QTR, MGR, GXR and NECR have a relatively small number of counties with the decreasing trend in eco-environmental vulnerability. The numbers of counties with mild vulnerability in the SCR and GXR decrease under RCP 4.5, 6.0 and 8.5 scenarios. The YRR show an increasing trend in the number of counties with

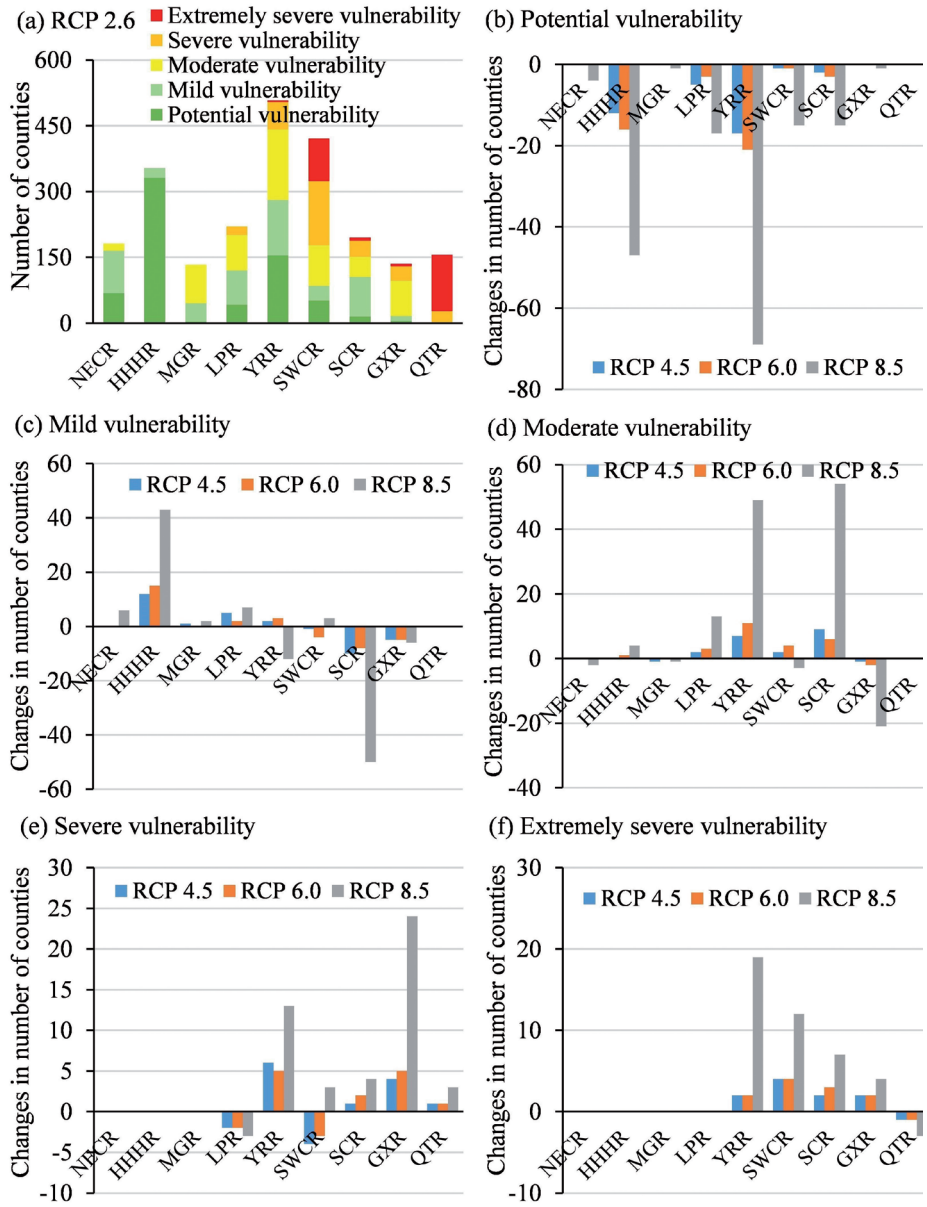

Fig. 3. Difference of environmental vulnerability grades under different scenarios. a) Distribution of environmental vulnerability grades in different agricultural zones under RCP 2.6; (b-f) Changes of environmental vulnerability grades for agricultural zones under RCP 4.5, 6.0 and 8.5 scenarios compared with that under RCP 2.6.

mild vulnerability under RCP 4.5 and 6.0 scenarios, while a decrease trend under RCP 8.5 scenarios. On the contrary, the SWCR presents a decreasing trend under RCP 4.5 and 6.0 scenarios, while an increasing trend under RCP 8.5. The numbers of counties with mild and potential vulnerability in the QTR keep constant under the four RCP scenarios. The rest four agricultural regions (NECR, HHHR, MGR, LPR) have an increasing trend in the number of counties with mild vulnerability as a whole. The YRR and SCR have the biggest increment in the number of counties with moderate vulnerability, especially under RCP 8.5. The GXR shows a decreasing trend in the number of counties with moderate vulnerability under RCP 4.5, 6.0 and 8.5 scenarios, and especially under RCP 8.5, the number of counties with moderate vulnerability is reduced by 20. The LPR has an obvious increase in the number of counties with moderate vulnerability, with an increase of 2, 3 and 13 counties under RCP 4.5, 6.0, and 8.5 scenarios, respectively. The numbers of counties with severe vulnerability increase under the high radiative forcing levels in many agricultural regions, such as the YRR, SCR, GXR and QTR. The number of counties with severe vulnerability increases most in the GXR under RCP 8.5, increased by 24. Under RCP 4.5 and 6.0 scenarios, the YRR has the largest increase in the number of counties with severe vulnerability. In terms of the number of counties with extremely severe vulnerability, except for the QTR showing a decreasing trend, the other regions have an increasing trend

(excluding the NECR, HHHR, MGR and LPR, which do not have extremely severe vulnerability). The SWCR has the largest increment in the number of counties with extremely severe vulnerability under RCP 4.5 and 6.0 scenarios. Under RCP 8.5, the YRR has the largest increment, increased by about 20 counties, followed by the SWCR, increased by 12 counties.

On the whole, with the increase of radiative farcing level, the number of counties with potential vulnerability shows a downward trend, and those of severe and extremely severe vulnerability show an upward trend. In addition, the numbers of counties with different vulnerability grades change largely under RCP 8.5 compared with those of other scenarios.

Dynamic Variations of Eco-Environmental Vulnerability

According to the statistics (Table 4), for the period 2020s-2050s, the vulnerability grade increases by 0.1055 on nationwide average under RCP 4.5, higher than those under other scenarios. By the 2090s, the increase in eco-environmental vulnerability under RCP 8.5 scenario was the most obvious, with an average increase of 1.0156 nationwide, far exceeding those of other three scenarios. RCP 2.6 scenario shows the smallest change in eco-environmental vulnerability, increasing by 0.0439. In other words, the eco-environmental vulnerability is the most stable under RCP 2.6 scenario, and under RCP 4.5 and 6.0 scenarios, the eco-environmental vulnerability shows different change in different stages. The eco-environmental vulnerability increases significantly in the late 21st century under RCP 8.5 scenario.

The eco-environmental vulnerability varies differently in space over time among scenarios (Fig. 4). Under RCP 2.6, areas showing gradual changing trend in vulnerability grade area mainly located in a small range, mainly distributed in the southern part of China and rising by 1 level. The number of counties with increasing trend in vulnerability grade in 2090s is slightly more than that of 2050s. Under RCP 4.5, areas with rising vulnerability level expand, which are still mainly located in the southern China in 2050s. By 2090s, these areas in the southern China with rising vulnerability level are contiguous in space. Meanwhile, some counties with rising vulnerability level appear in the northwestern China. Under RCP 6.0, the difference of eco-environmental vulnerability between 2050s and 2090s gets widened. In the 2050s, the number of counties showing rising eco-environmental vulnerability grade is similar to that of RCP 2.6 scenario. By the 2090s, the vulnerability grades of a large contiguous areas increase, and the increases by 2 levels are obvious in many areas. Under RCP 8.5, the changes of eco-environmental vulnerability in 2050s are slightly smaller than that under RCP 4.5. Areas with rising vulnerability grade are mainly located in central and southern China, and a small number of counties in Xinjiang also show a rising trend in vulnerability grade. By 2090s, the vulnerability grades increase most obviously, mainly distributed in the east of Hu's Line. Areas with an increase by 2 levels expand much, accounting for almost half of the areas where the vulnerability grade changes, and are mainly distributed in the central region.

Table 4. Changes of vulnerability grades in China under RCP scenarios.

scenario	2020s-2050s	2020s-2090s
RCP 2.6	0.0261	0.0439
RCP 4.5	0.1055	0.2097
RCP 6.0	0.0104	0.4685
RCP 8.5	0.0795	1.0156

Trends of Eco-Environmental Vulnerability

The trend variation and change rate of eco-environmental vulnerability under the four scenarios were displayed in Fig. 5. According to MK trend test, eco-environmental vulnerability shows upward tendency overall, and some areas with significant downward trend only appear under RCP 2.6 scenario, mainly located in Inner Mongolia and Qinghai. Obvious differences in tendency exist among scenarios. Under RCP 2.6 scenario, eco-environmental vulnerability has no significant change in most areas. Along with the rise of the radiative forcing level, areas with significant upward trend expand obviously; as a result, eco-environmental vulnerability under RCP 8.5 scenario increases in a large area. In terms of regional differences, the northwestern and southeastern regions affected greatly by the climate change, while the southwestern region shows no significant change in eco-environmental vulnerability.

As for the change rate of eco-environmental vulnerability, the average increments are 0.0004, 0.0022, 0.0037 and 0.0092 per decade under RCP 2.6, 4.5, 6.0 and 8.5 scenarios. The change rate increases as the radiative forcing level rises. Specifically, under RCP 2.6, large areas show a slowly increasing trend, and areas with relatively fast growth primarily appear in central region, such as continuous regions of Henan-Anhui-Hubei, with the highest change rate of 0.0029 per decade in Pingdingshan city. Under RCP 4.5, areas with decreasing trend shrink and are distributed dispersedly. The southeastern region shows a relatively fast growth in eco-environmental vulnerability, with a change rate above 0.002. Areas with a growth rate of more than 0.005 mainly appear in Hunan, Jiangxi and Guangxi. Areas in Xinxiang and western Inner Mongolia also show a relative fast increase in eco-environmental vulnerability. Under RCP 6.0, the central region and the northwestern region are still the most well-marked

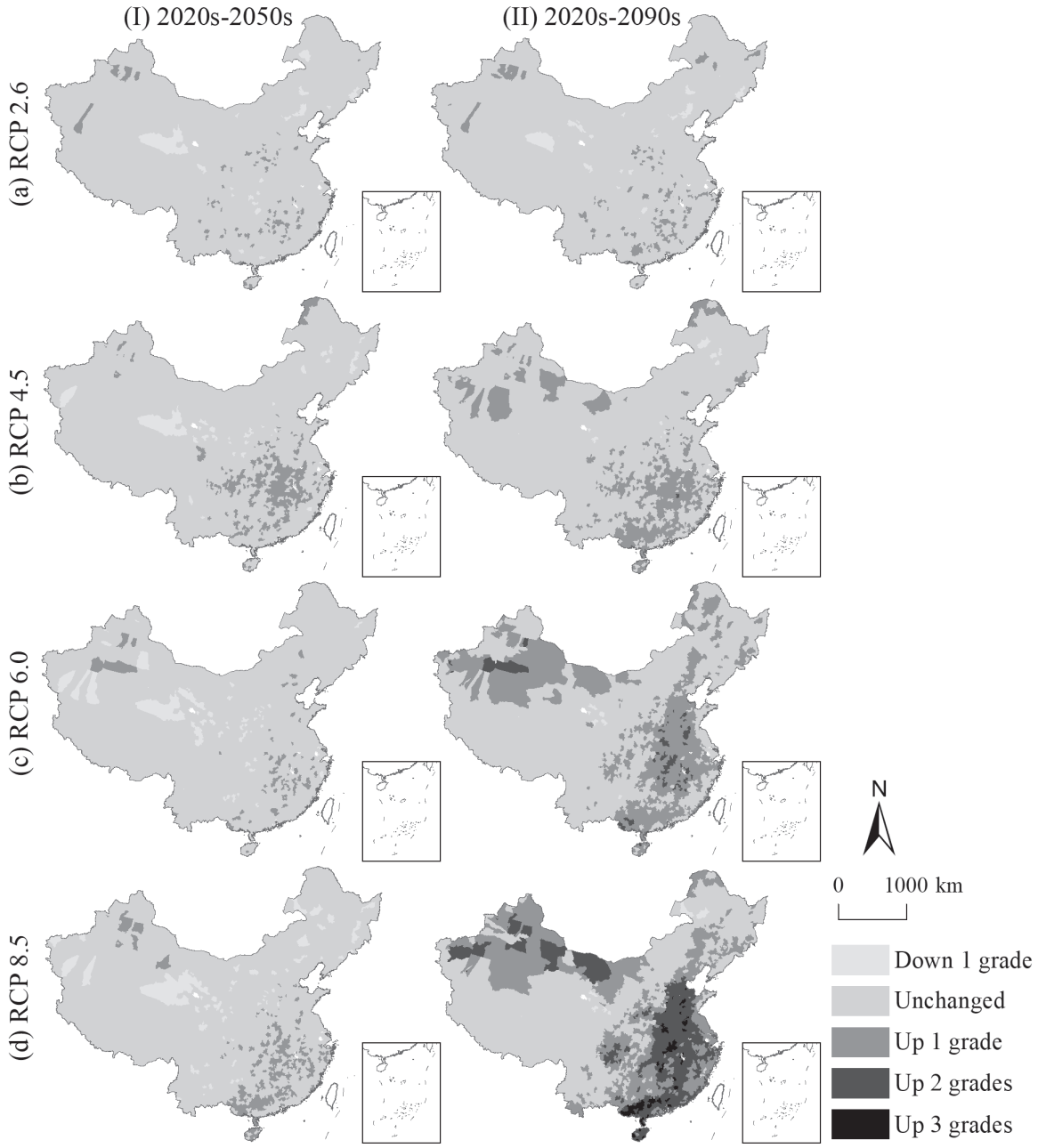

Fig. 4. Spatial distribution of changes in environmental vulnerability grades under RCP scenarios for 2050s and 2090s, respectively.

areas with high growth rate of eco-environmental vulnerability, and growth rate has exceeded 0.01 in Hunan, Jiangxi and Guangxi. Under RCP 8.5, the growth rates of eco-environmental vulnerability accelerate on a national scale. Large and continuous areas in northwestern and southeastern regions show a fast growth, and numerous counties will experience a rapid growth of exceeding 0.02 per decade.

Discussion

In terms of data source, the simulated atmospheric climate data were utilized in this study, including five models (MIROC-ESM-CHEM, NorESl-M, IPSL-CM5A-LR, GFDL-ESM 2M and HadGEM2-ES). All of them originated from the ISI-MIP, which have been validated effectively [61, 62], and widely used in studies related climate change [59, 60, 63, 64]. In order to reduce the model uncertainty, we averaged these five models at daily time steps to eliminate outliers and then calculated indicators used for our assessment index system.

Numerous studies have been conducted on a regional scale, such as Daxing'anling [27], the middle of the Inner Mongolia [65], counties within Mu Us Desert [66], Huainai City [67], Southern Shaanxi [68], Xianshui River Basin [42], Yellow River Basin [41], and so on. The majority of these studies aimed at a specific region with a small area, and the Intra-regional differences

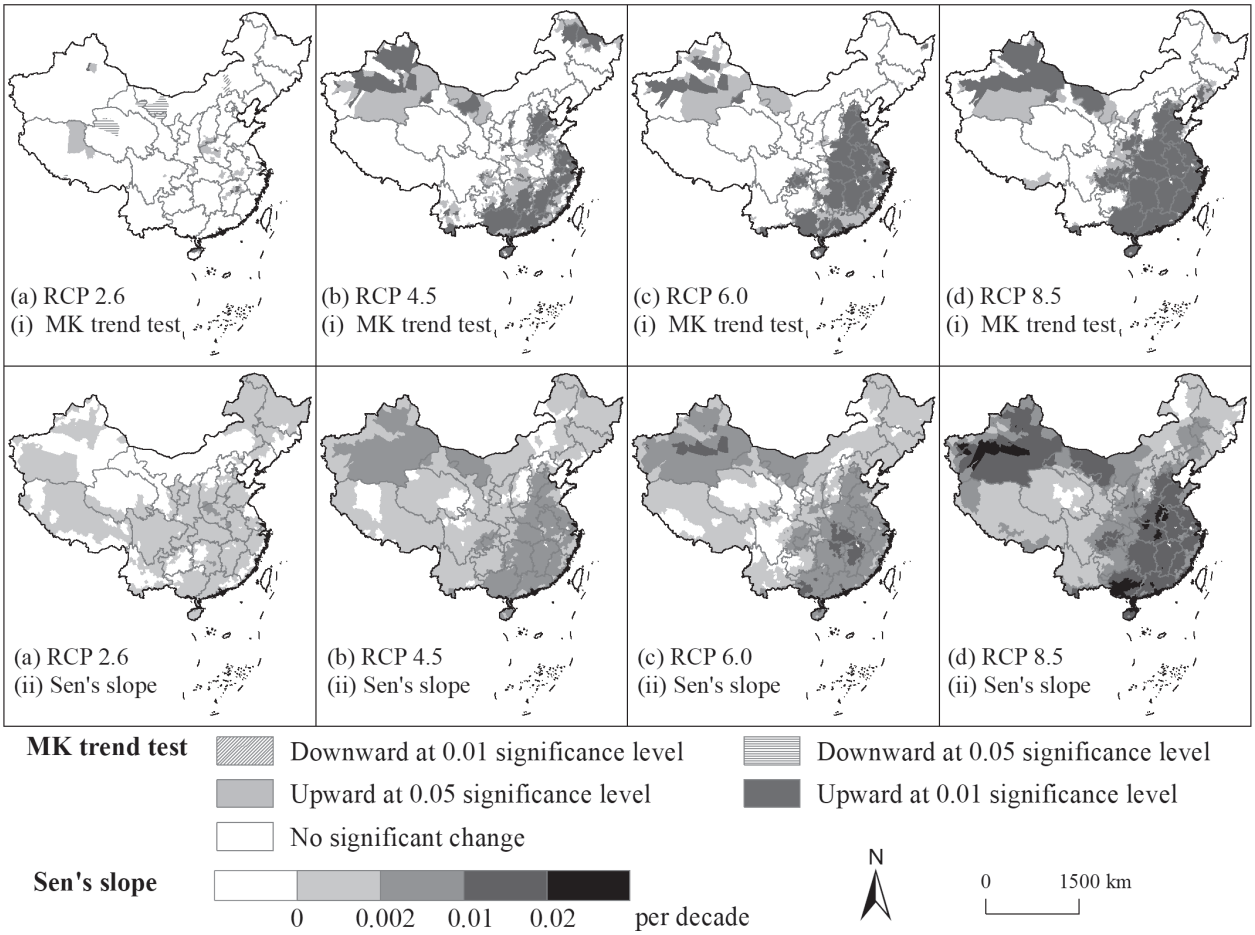

Fig. 5. Trend of environmental vulnerability grades under RCP scenarios.

could not be compared with our results. The assessment result in Yellow River Basin showed that the north region (roughly equivalent to the north Loess Plateau) had a higher degree of eco-environmental vulnerability than that of south region, which is consistent with our result. However, the eco-environmental vulnerability is still lower than that of the west China, which implied that vulnerability assessment at national scale is essential to understand the overall ecological condition for China. In addition, some researchers conducted vulnerability assessment at global or national scale. For example, Nguyen and Liou [13] mapped the eco-environmental vulnerability for the world. Results showed that China has the maximum area with high level of vulnerability, and the southeastern China has a high degree of vulnerability, which is concordant with our result. He et al. [25] constructed an ecological vulnerability assessment framework integrating natural, social, economic, environmental pollution and human health elements in 31 provinces of China. Results showed that Xinjiang has a vulnerable ecological environment, and our result basically verified this point. However, the Qinghai-Tibet Plateau Region showed an inconsistent assessment result, which is likely due to the different evaluation system designed according to the different research objective. Additionally, the assessment result for 31 provinces lack in a detailed spatial map, which leads to the same degree of vulnerability southern China. Consequently, it is meaningful that this study evaluated the eco-environmental vulnerability for counties in China.

The study identified areas with highly vulnerable eco-environment across the country, as well as areas that are sensitive to climate change. In order to protect the ecological environment, the corresponding control measures should be put forward targeted the certain area. The western region has a high degree of eco-environment vulnerability, while its sensitivity to climate change is low, with a stable vulnerability under climate change scenarios. However, the southeast region has a relatively low degree of eco-environment vulnerability, while it is highly sensitive to climate change. Therefore, from the perspective of climate change, the southeast region should be the most concerned region.

Conclusions

The ecological security has an important influence on regional sustainable development and management. Global warming significantly affects terrestrial

ecosystems from many aspects, and therefore it is necessary to evaluate the future trend of eco-environmental vulnerability under the background climate change. In this study, we constructed an assessment indicator system to evaluate the future eco-environmental vulnerability for China national scale, the spatial and temporal trends are predicted under four RCP scenarios. The main conclusions are as follows:

(1) In terms of the spatial distribution of eco-environmental vulnerability, areas with higher vulnerability are mainly located in the western and appear at the junction of provinces in southern China, while the eco-environmental vulnerability is generally low in the eastern region and the coastal areas of South China.

(2) The degree of eco-environmental vulnerability increases as the radiative forcing level rises, especially in Loess Plateau, Southwestern China and Gan-Xin regions where the eco-environmental vulnerability increases obviously under the high emission scenario. By contrast, the Northeast China is the most stable with less changes, followed by Inner Mongolia and the Great Wall region.

(3) In terms of dynamic variations, the changes in eco-environmental vulnerability vary among different scenarios. Areas with an upward trend in vulnerability grade are mainly located in southeastern and northwestern China. It is obvious that the eco-environmental vulnerability in North China Plain shows a significant upward trend under RCP 8.5 scenario. By comparison between the two time periods, the increases in vulnerability grades in 2090s are more significantly higher than that in 2050s, especially under RCP 8.5 scenario, where the vulnerability grade rises by 2 levels in a large-scale area.

(4) The trends of eco-environmental vulnerability show upward tendency overall and there is an obvious difference among different scenarios. The eco-environmental vulnerability has no significant change under RCP 2.6 scenario, while under other scenarios, large areas show significant upward trend, especially the RCP 8.5 scenario. The northwestern and southeastern regions have the biggest changes in eco-environmental vulnerability, while the southwestern region shows no significant changes. The change rates of eco-environmental vulnerability are the highest under RCP 8.5 scenario, with large and continuous areas showing fast growth.

Acknowledgments

This study was supported by the National Natural Science Foundation of China (No. 42001220; 42171182), Foundation of Henan Normal University for Young Scholars (No. 2021QK24), Soft Science Research Project of Henan Province (212400410310; 222400410427), and Innovation Team of Philosophy and Social Science of Colleges and Universities in Henan Province (No. 2021-CXTD-04).

Conflict of Interest

The authors declare no conflict of interest.

References

1. ZHENG Y., WANG S., CAO Y., SHI J, QU Y, LI L., ZHAO T., NIU Z., YANG R., GONG P. Assessing the ecological vulnerability of protected areas by using Big Earth Data. International Journal of Digital Earth, **14** (11), 1624, **2021**.
2. VILLA F., MCLEOD H. Environmental vulnerability indicators for environmental planning and decision-making: guidelines and applications. Environmental Management, **29**, 335, **2002**.
3. CHANG C.L. Evaluation of basin environmental vulnerability: the weighted method compared to the compromise method. International Journal of Environmental Science and Technology, **10**, 1051, **2013**.
4. WEN J.F., HOU K. Research on the progress of regional ecological security evaluation and optimization of its common limitations. Ecological Indicators, **127**, 107797, **2021**.
5. GOETZ S.J., BUNN A.G., FISKE G.J., HOUGHTON R.A. Satellite-observed photosynthetic trends across Boreal North America associated with climate and fire disturbance. Proceeding Academy of Sciences of the United States of America, **102** (38), 13521, **2005**.
6. GUO B., ZHOU Y., ZHU J., LIU W., WANG F., WANG L., YAN F., WANG F., YANG G., LUO W., JIANG L. Spatial patterns of ecosystem vulnerability changes during 2001-2011 in the three-river source region of the Qinghai-Tibetan Plateau, China. Journal of Arid Land, **8**, 23, **2016**.
7. HONG W., JIANG R., YANG C., ZHANG F., SU M., LIAO Q. Establishing an ecological vulnerability assessment indicator system for spatial recognition and management of ecologically vulnerable areas in highly urbanized regions: A case study of Shenzhen, China. Ecological Indicators, **69**, 540, **2016**.
8. SAHOO S., DHAR A., KAR A. Environmental vulnerability assessment using Grey Analytic Hierarchy Process based model. Environmental Impact Assessment Review, **56**, 145, **2016**.
9. YANG G., CHEN Z. RS-based fuzzy multiattribute assessment of eco-environmental vulnerability in the source area of the Lishui River of northwest Hunan Province, China. Natural Hazards, **78**, 1145, **2015**.
10. LIU Y., YANG S., HAN C., NI W., ZHU Y. Variability in Regional Ecological Vulnerability: A Case Study of Sichuan Province, China. International Journal of Disaster Risk Science, **11**, 696, **2020**.
11. HOU K., LI X., ZHANG J. GIS analysis of changes in ecological vulnerability using a SPCA model in the Loess Plateau of Northern Shaanxi, China. International Journal of Environmental Research and Public Health, **12** (4), 4292, **2015**.
12. ZHANG F., LIU X., ZHANG J., WU R., MA Q., CHEN Y. Ecological vulnerability assessment based on multi-sources data and SD model in Yinma River Basin, China. Ecological Modelling, **349**, 41, **2017**.

13. NGUYEN K., LIOU Y. Global mapping of eco-environmental vulnerability from human and nature disturbances. Science of the Total Environment, **664**, 995, **2019**.
14. CHAPIN III F.S., MCGUIRE A.D., RANDERSON J., PIELKE SR. R., BALDOCCHI D., HOBBIE S.E., ROULET N., EUGSTER W., KASISCHKE E., RASTETTER E.B., ZIMOV S.A., RUNNING S.W. Arctic and boreal ecosystems of western North America as components of the climate system. Global Change Biology, **6** (S1), 211, **2000**.
15. IPCC. Climate Change 2007: the Physical Science Basis. Working Group I to the Fifth assessment report of the Intergovernmental Panel on Climate Change. Cambridge University Press: Cambridge, United Kingdom, **2007**.
16. WESTERLING A.L., TURNER M.G., SMITHWICK E.A.H., ROMME W.H., RYAN M.G. Continued warming could transform Greater Yellowstone fire regimes by mid-21st century. Proceeding Academy of Sciences of the United States of America, **108** (32), 13165, **2011**.
17. HAMED M.M., NASHWAN M.S., SHAHID S., ISMAIL T., WANG X., DEWAN A.D., ASADUZZAMAN M. Inconsistency in historical simulations and future projections of temperature and rainfall: A comparison of CMIP5 and CMIP6 models over Southeast Asia. Atmospheric Research, **265**, 105927, **2022**.
18. KANG S., ELTAHIR E.A.B. North China Plain threatened by deadly heatwaves due to climate change and irrigation. Nature Communications, **9**, 2894, **2018**.
19. NASHWAN M.S., SHAHID S. Future precipitation changes in Egypt under the 1.5 and 2.0ºC global warming goals using CMIP6 multimodel ensemble. Atmospheric Research, **265**, 105908, **2022**.
20. ZIARH G.F., ASADUZZAMAN M., DEWAN A., NASHWAN M. S., SHAHID S. Integration of catastrophe and entropy theories for flood risk mapping in peninsular Malaysia. Journal of Flood Risk Management, **14**, e12686, **2021**.
21. SHAO H., SUN X., TAO S., XIANG Z., XIAN W. Environmental vulnerability assessment in middle-upper reaches of Dadu River Watershed using Projection Pursuit Model and GIS. carpathian journal of earth and environmental sciences, **10**, 133, **2015**.
22. BERRY P.M., ROUNSEVELL M.D.A., HARRISON P.A., AUDSLEY E. Assessing the vulnerability of agricultural land use and species to climate change and the role of policy in facilitating adaptation. Environmental Science & Policy, **9**, 189, **2006**.
23. RUIJVEN B.J.V., LEVY M.A., AGRAWAL A., BIERMANN F., BIRKMANN J., CARTER T.R., EBI K.L., GARSCHAGEN M., JONES B., JONES R., KEMP-BENEDICT E., KOK M., KOK K., LEMOS M. C., LUCAS P. L., ORLOVE B., PACHAURI S., PARRIS T., PATWARDHAN A., PETERSEN A., PRESTON B.L., RIBOT J., ROTHMAN D.S., SCHWEIZER V.J. Enhancing the relevance of Shared Socioeconomic Pathways for climate change impacts, adaptation and vulnerability research. Climatic Change, **122**, 481, **2014**.
24. WOLF S. Vulnerability and risk: comparing assessment approaches. Natural Hazards, **61** (3), 1099, **2012**.
25. HE L., SHEN J., ZHANG Y. Ecological vulnerability assessment for ecological conservation and environmental management. Journal of Environmental Management, **206**, 1115, **2018**.
26. JIANG Y., SHI B., SU G., LU Y., LI Q., MENG J., DING Y., SONG S., DAI L. Spatiotemporal analysis of ecological vulnerability in the Tibet Autonomous Region based on a pressure-state-response-management framework. Ecological Indicators, **130**, 108054, **2021**.
27. ZOU T., YOSHINO K. Environmental vulnerability evaluation using a spatial principal components approach in the Daxing'anling region, China. Ecological Indicators, **78**, 405, **2017**.
28. YU X., LI Y., XI M., KONG F., PANG M., YU Z. Ecological vulnerability analysis of Beidagang National Park, China. Frontiers of Earth Science, **13**, 385, **2019**.
29. LIU H., WILLEMS P., BAO A., WANG L., CHEN X. Effect of climate change on the vulnerability of a socio-ecological system in an arid area. Global and Planetary Change, **137**, 1, **2016**.
30. BAI J., LI J., BAO A., Chang C. Spatial-temporal variations of ecological vulnerability in the Tarim River Basin, Northwest China. Journal of Arid Land, **13**, 814, **2021**.
31. NICHOLLS R.J. Analysis of global impacts of sea-level rise: a case study of flooding. Physics & Chemistry of the Earth, **27**, 1455, **2002**.
32. WALTHER G., POST E., CONVEY P., MENZEL A., PARMESAN C., BEEBEE T.J.C., FROMENTIN J., HOEGH-GULDBERG O., BAIRLEIN F. Ecological responses to recent climate change. Nature, **416**, 389, **2002**.
33. GAO J., NICKUM J.E., PAN Y. An assessment of flood hazard vulnerability in the Dongting Lake Region of China. Lakes & Reservoirs: Science, Policy and Management for Sustainable Use, **12**, 27, **2007**.
34. SMITH M.D. The ecological role of climate extremes: current understanding and future prospects. Journal of Ecology, **99**, 651, **2011**.
35. MCLEMAN R.A. Settlement abandonment in the context of global environmental change. Global Environmental Change, **21**, S108, **2011**.
36. SHIRU M.S., SHAHID S., DEWAN A., CHUNG E.S., ALIAS N., AHMED K., HASSAN Q. Projection of meteorological droughts in Nigeria during growing seasons under climate change scenarios. Scientific Reports, **10**: 10107, **2020**.
37. RAHMAN M., CHEN N., ELBELTAGI A., ISLAM M.M., ALAM M., POURGHASEMI H. R., TAO W., ZHANG J., TIAN S., FAIZ H., BAIG M.A., DEWAN A. Application of stacking hybrid machine learning algorithms in delineating multi-type flooding in Bangladesh. Journal of Environmental Management, **295**, 113086, **2021**.
38. MALLARI A.E.C. Climate Change Vulnerability Assessment in the Agriculture Sector: Typhoon Santi Experience. Procedia - Social and Behavioral Sciences, **216**, 440, **2016**.
39. KUMAR P., GENELETTI D., NAGENDRA H. Spatial assessment of climate change vulnerability at city scale: A study in Bangalore, India. Land Use Policy, **58**, 514, **2016**.
40. APREDA C., D' AMBROSIO V., DI MARTINO F. A climate vulnerability and impact assessment model for complex urban systems. Environmental Science & Policy, **93**, 11, **2019**.
41. WANG S.Y., LIU J.S., YANG C.J. Eco-Environmental Vulnerability Evaluation in the Yellow River Basin, China. Pedosphere, **18** (2), 171, **2008**.
42. SHAO H., SUN X., WANG H., ZHANG X., XIANG Z., TAN R., CHEN X., XIAN W., QI J. A method to the impact assessment of the returning grazing land to grassland project on regional eco-environmental vulnerability. Environmental Impact Assessment Review, **56**, 155, **2016**.

43. ZHAO J.C., JI G.X., TIAN Y., CHEN Y., WANG Z. Environmental vulnerability assessment for mainland China based on entropy method. Ecological Indicators, **91**, 410, **2018**
44. WU S.H., DAI E.F., HUANG M., SHAO X., LI S., TAO B. Ecosystem vulnerability of China under B2 climate scenario in the 21st century. Chinese Science Bulletin, **52**, 811, **2007**.
45. ZHAO D.S., WU S.H. Vulnerability of natural ecosystem in China under regional climate scenarios: An analysis based on eco-geographical regions. Journal of Geographical Sciences, **24** (2), 237, **2014**.
46. SHUKLA R., CHAKRABORTY A., JOSHI P.K. Vulnerability of agro-ecological zones in India under the earth system climate model scenarios. Mitigation & Adaptation Strategies for Global Change, **22**, 399, **2017**.
47. UDDIN M.N., SAIFUL ISLAM A.K.M., BALA S.K., TAREKUL ISLAM G.M., ADHIKARY S., SAHA D., HAQUE S., FAHAD M.G.R., AKTER R. Mapping of climate vulnerability of the coastal region of Bangladesh using principal component analysis. Applied Geography, **102**, 47, **2019**.
48. SAHOO S., DHAR A., DEBSARKAR A., KAR A. Future scenarios of environmental vulnerability mapping using grey analytic hierarchy process. Natural Resources Research, **28** (4), 1461, **2019**.
49. FU J., LIU J., WANG X., ZHANG M., CHEN W., CHEN B. Ecological risk assessment of wetland vegetation under projected climate scenarios in the Sanjiang Plain, China. Journal of Environmental Management, **273**, 111108, **2020**.
50. XU K., WANG X., JIANG C., SUN O.J. Assessing the vulnerability of ecosystems to climate change based on climate exposure, vegetation stability and productivity. Forest Ecosystems, **7**, 23, **2020**.
51. XU X., LIN H., HOU L., YAO X. An assessment for sustainable developing capability of integrated agricultural regionalization in China. Chinese Geographical Science, **12**, 1, **2002**.
52. HAGEMANN S., CHEN C., HAERTER J.O., HEINKE J., GERTEN D., PIANI C. Impact of a statistical bias correction on the projected hydrological changes obtained from three GCMs and two hydrology models. Journal of Hydrometeorology, **12** (4), 556, **2011**.
53. PIANI C., WEEDON G.P., BEST M., GOMES S.M., VITERBO P., HAGEMANN S., HAERTER J.O. Statistical bias correction of global simulated daily precipitation and temperature for the application of hydrological models. Journal of Hydrology, **395**, 199, **2010**.
54. HEMPEL S., FRIELER K., WARSZAWSKI L., SCHEWE J., PIONTEK F. A trend-preserving bias correction – the ISI-MIP approach. Earth System Dynamics, **4**, 219, **2013**.
55. HAYAT H., AKBAR T.A., TAHIR A.A., HASSAN Q.K., DEWAN A., IRSHAD M. Simulating current and future river-flows in the Karakoram and Himalayan regions of Pakistan using snowmelt-runoff model and RCP scenarios. Water, **11**, 761, **2019**.
56. TULADHAR D., DEWAN A., KUHN M., CORNER R.J. The influence of rainfall and land use/land cover changes on river discharge variability in the mountainous catchment of the Bagmati River. Water, **11**, 2444, **2019**.
57. TILLACK A., CLASEN A., KLEINSCHMIT B., FÖRSTER M. Estimation of the seasonal leaf area index in an alluvial forest using high-resolution satellite-based vegetation indices. Remote Sensing of Environment, **141**: 52, **2014**.
58. HAN B., LIU H., WANG R. Urban ecological security assessment for cities in the Beijing-Tianjin-Hebei metropolitan region based on fuzzy and entropy methods. Ecological Modelling, **318**, 217, **2015**.
59. ZHAO J.C., XIA H.B., YUE Q., WANG Z. Spatiotemporal variation in reference evapotranspiration and its contributing climatic factors in China under future scenarios. International Journal of Climatology, **40** (8), 3813, **2020**.
60. ZHAO J.C., LIU Q.Q., LU H.L., WANG Z., ZHANG K., ZHANG K., WANG P. Future droughts in China using the standardized precipitation evapotranspiration index (SPEI) under multi-spatial scales. Natural Hazards, **109**, 615, **2021**.
61. WU S.H., PAN T., LIU Y.H., DENG H., JIAO K., LU Q., FENG A.Q., YUE X.L., YIN Y.H., ZHAO D.S., GAO J.B. Comprehensive climate change risk regionalization of China. Acta Geographica Sinica, **72** (1), 3, **2017**.
62. ZHAO J.C., WANG Z. Future trends of water resources and influences on agriculture in China. PLoS ONE, **15** (4), e0231671, **2020**.
63. PORTMANN F.T., DÖLL P., EISNER S., FLÖRKE M. Impact of climate change on renewable groundwater resources: assessing the benefits of avoided greenhouse gas emissions using selected CMIP5 climate projections. Environmental Research Letters, **8** (2), 024023 **2013**.
64. DAVIE J.C.S., FALLOON P.D., KAHANA R., DANKERS R., BETTS R., PORTMANN F.T., WISSER D., CLARK D.B., ITO A., MASAKI Y., NISHINA K., FEKETE B., TESSLER Z., WADA Y., LIU X., TANG Q., HAGEMANN S., STACKE T., PAVLICK R., SCHAPHOFF S., GOSLING S.N., FRANSSEN W., ARNELL N. Comparing projections of future changes in runoff and water resources from hydrological and ecosystem models in ISI-MIP. Earth System Dynamics, **4** (1), 279, **2013**.
65. JIANG L., HUANG X., WANG F., LIU Y., AN P. Method for evaluating ecological vulnerability under climate change based on remote sensing: A case study. Ecological Indicators, **85**, 479, **2018**.
66. LV X., XIAO W., ZHAO Y., ZHANG W., LI S., SUN H. Drivers of spatio-temporal ecological vulnerability in an arid, coal mining region in Western China. Ecological Indicators, **106**, 105475, **2019**.
67. HE G., BAO K., WANG W., ZHU Y., LI S., JIN L. Assessment of ecological vulnerability of resource-based cities based on entropy-set pair analysis. Environmental Technology, **42** (12), 1874, **2021**.
68. HOU K., TAO W., CHANG Y., ZHANG Y., LI X., CHEN P. A feasible method for the division of ecological vulnerability and its driving forces in Southern Shaanxi. Journal of Cleaner Production, **205**, 619, **2018**.